Structural Perturbation of the Carboxylate Ligands to the Manganese Cluster upon Ca^{2+}/Sr^{2+} Exchange in the S-State Cycle of Photosynthetic Oxygen Evolution As Studied by Flash-Induced FTIR Difference Spectroscopy†

Hiroyuki Suzuki,‡ Yuta Taguchi,‡ Miwa Sugiura,§ Alain Boussac,|| and Takumi Noguchi*,‡

Institute of Materials Science, University of Tsukuba, Tsukuba, Ibaraki 305-8573, Japan, Department of Plant Bioscience, School of Life and Environmental Sciences, Osaka Prefecture University, 1-1 Gakuen-cho, Sakai, Osaka 599-8531, Japan, and Service de Bioénergétique, DBJC, URA CNRS 2096, CEA Saclay, 91191 Gif-sur-Yvette, France

Received June 21, 2006; Revised Manuscript Received September 11, 2006

ABSTRACT: A Ca^{2+} ion is an indispensable element in the oxygen-evolving Mn cluster in photosystem II (PSII). To investigate the structural relevance of Ca^{2+} to the Mn cluster, the effects of Sr^{2+} substitution for Ca^{2+} on the structures and reactions of ligands to the Mn cluster during the S-state cycle were investigated using flash-induced Fourier transform infrared (FTIR) difference spectroscopy. FTIR difference spectra representing the four S-state transitions, $S_1 \rightarrow S_2$, $S_2 \rightarrow S_3$, $S_3 \rightarrow S_0$, and $S_0 \rightarrow S_1$, were recorded by applying four consecutive flashes either to PSII core complexes from *Thermosynechococcus elongatus* or to PSII-enriched membranes from spinach. The spectra were also recorded using biosynthetically Sr^{2+}-substituted PSII core complexes from *T. elongatus* and biochemically Sr^{2+}-substituted PSII membranes from spinach. Several common spectral changes upon Sr^{2+} substitution were observed in the COO^- stretching region of the flash-induced spectra for both preparations, which were best expressed in Ca^{2+}-minus-Sr^{2+} double difference spectra. The significant intensity changes in the symmetric COO^- peaks at ∼1364 and ∼1418 cm^{-1} at the first flash were reversed as opposite intensity changes at the third flash, and the slight shift of the ∼1446 cm^{-1} peak at the second flash corresponded to the similar but opposite shift at the fourth flash. Analyses of these changes suggest that there are at least three carboxylate ligands whose structures are significantly perturbed by Ca^{2+}/Sr^{2+} exchange. They are (1) the carboxylate ligand having a bridging or unidentate structure in the S_2 and S_3 states and perturbed in the $S_1 \rightarrow S_2$ and $S_3 \rightarrow S_0$ transitions, (2) that with a chelating or bridging structure in the S_1 and S_0 states and perturbed also in the $S_1 \rightarrow S_2$ and $S_3 \rightarrow S_0$ transitions, and (3) that with a chelating structure in the S_3 and S_0 states and changes in the $S_2 \rightarrow S_3$ and $S_0 \rightarrow S_1$ transitions. Taking into account the recent FTIR studies using site-directed mutagenesis and/or isotope substitution [Chu et al. (2004) *Biochemistry 43*, 3152−3116; Kimura et al. (2005) *J. Biol. Chem. 280*, 2078−2083; Strickler et al. (2006) *Biochemistry 45*, 8801−8811], it was concluded that these carboxylate groups do not originate from either D1-Ala344 (C-terminus) or D1-Glu189, which are located near the Ca^{2+} ion in the X-ray crystallographic model of the Mn cluster. It was thus proposed that if the X-ray model is correct, the above carboxylate groups sensitive to Sr^{2+} substitution are ligands to the Mn ions strongly coupled to the Ca^{2+} ion rather than direct ligands to Ca^{2+}.

Oxygen evolution in plants and cyanobacteria is performed at the oxygen-evolving center (OEC)[1] in the photosystem II protein complexes (*1*, *2*). The chemical identity of OEC is the so-called Mn cluster, which consists of four Mn ions, embedded in the protein matrix (*3*−*5*). Molecular oxygen is released as a result of four-electron oxidation of two water molecules, which is accomplished through a light-driven cycle of five intermediates called S states (S_0−S_4). Among these intermediates, the S_1 state is the most dark stable, and successive four-flash illumination advances S_1 to S_2, S_2 to S_3, S_3 to S_0, and S_0 to S_1. Molecular oxygen is released upon illumination on the S_3 state via the unstable S_4 state. It has been known that Ca^{2+} is an indispensable cofactor for oxygen evolution and is located in the vicinity of the Mn ions (*1*, *6*, *7*). EXAF studies have shown that the distance between the Ca^{2+} ion and the Mn ions is about 3.4 Å (*3*). The recent X-ray crystal structures of the PSII core complexes of the cyanobactrium *Thermosynechococcus elongatus* at 3.5 and 3.0 Å resolutions (*8*, *9*) indeed showed that one Ca^{2+} ion is involved in the electron density of the Mn cluster. It was also shown that D1-Asp170, D1-Glu189, D1-Glu333, D1-Asp342, D1-Ala344 (C-terminus), CP43-Glu354, and D1-His332 are candidates for the ligands to the Mn and Ca ions

† This study was supported by Grants-in-Aid for Scientific Research (17GS0314 and 18570145) from the Ministry of Education, Science, Sports, Culture, and Technology, by JSPS and CNRS under the Japan−France Research Co-operative Program Japan, and by Special Research Project "NanoScience" at the University of Tsukuba.

* Corresponding author. Phone: +81-29-853-5126. Fax: +81-29-853-4490. E-mail: tnoguchi@ims.tsukuba.ac.jp.

‡ University of Tsukuba.

§ Osaka Prefecture University.

|| Service de Bioénergétique, DBJC.

[1] Abbreviations: FTIR, Fourier transform infrared; Mes, 2-(*N*-morpholino)ethanesulfonic acid; OEC, oxygen-evolving center; PpBQ, phenyl-*p*-benzoquinone; PSII, photosystem II.

10.1021/bi061232z CCC: $33.50
Published on Web 10/20/2006

(*8*, *9*), being consistent with mutagenesis studies (*1*, *4*). The relatively low resolutions of these X-ray structures (*8*, *9*) and the high Mn^{2+} content (*10*, *11*), however, could not definitely determine the core structure of the Mn_4Ca cluster as well as the detailed ligand structures. The Ca^{2+} ion can be replaced with a wide range of metal ions (*7*, *12*−*19*). Among them, only Sr^{2+} can restore the O_2-evolving activity (*13*−*15*). This indicates that Ca^{2+} is directly involved in the chemical mechanism of oxygen evolution, rather than only a structural component of OEC (*7*, *12*). Various models of the mechanism involving the role of Ca^{2+} have been proposed (*2*, *7*, *20*−*22*). Indeed, a recent study of mass spectrometry showed that the slow phase of substrate exchange is significantly affected by Sr^{2+} substitution, indicating that Ca^{2+} is inherently involved in the binding of a substrate water molecule (*23*).

To investigate the detailed structures and molecular reactions of the redox cofactors in photosystem II, light-induced FTIR difference spectroscopy has been used as a powerful method (*24*). As for the oxygen-evolving reactions, FTIR difference spectra of OEC upon the individual S-state transitions have been obtained by applying flashes to the PSII samples in the presence of exogenous electron acceptors (*25*−*27*). Using this technique, the structures and reactions of the carboxylate (*28*−*35*) and His (*36*, *37*) ligands to the Mn cluster, substrate water molecules (*38*, *39*), and the Mn−O−Mn bonds (*40*, *41*) have been studied. In particular, the coupled asymmetric and symmetric COO^- stretching vibrations of carboxylate groups provide several strong features at 1600−1450 and 1450−1300 cm^{-1}, respectively, being consistent with the presence of five to six carboxylate ligands to the Mn cluster as proposed by the X-ray crystallographic studies (*8*, *9*). Because the frequency gap between the asymmetric and symmetric vibrations provides information about the coordination structure of carboxylate (*42*−*44*), these COO^- bands are very useful to characterize the structures and reactions of the carboxylate ligands to the Mn cluster.

In this study, we have investigated the ligand structure of the Mn cluster relevant to the Ca^{2+} ion, especially focusing on the carboxylate ligands, using flash-induced FTIR difference spectroscopy. For this purpose, we have examined the effects of Ca^{2+}/Sr^{2+} exchange on the FTIR difference spectra of individual S-state transitions. FTIR measurements of Sr^{2+}-substituted PSII samples have been performed mainly on the $S_1 \rightarrow S_2$ transition (*45*−*49*). Although one group (*48*, *49*) recently attempted to measure the FTIR spectra of Sr^{2+}-substituted PSII during the S-state cycle, the reactions after the S_3 state were inhibited in the PSII preparation used.[2] Thus, the effects of Sr^{2+} substitution on all of the S-state transitions have not been studied yet. In the present experiments, we used both the PSII core complexes from the cyanobacterium *T. elongatus* and the PSII-enriched membranes from spinach. In addition, two different electron acceptors, ferricyanide and PpBQ, were used for the *T. elongatus* sample. These measurements using different samples and measuring conditions can distinguish true features from possible artifacts, which are sometimes problematic in detecting subtle signal changes by a certain perturbation of the sample. Several common band changes upon Sr^{2+} substitution were observed in the COO^- region of the spectra during the S-state cycle. These band changes were analyzed using the criteria for determining the coordination structures and discussed in light of the previous FTIR studies for the carboxylate ligands and the X-ray crystallographic model of the Mn cluster.

MATERIALS AND METHODS

The PSII core complexes of *T. elongatus*, in which the carboxyl terminus of the CP43 subunit was genetically His-tagged, were purified using Ni^{2+}-affinity column chromatography as previously described (*50*). The core complexes in which Ca^{2+} was replaced with Sr^{2+} (Sr^{2+}−PSII) were prepared from *T. elongatus* cells that were grown in a DTN medium containing $SrCl_2$ instead of $CaCl_2$ (*15*). The core complexes were suspended in a pH 6.5 buffer (buffer A: 40 mM Mes, 15 mM $MgCl_2$, 15 mM $CaCl_2$, 1 M betaine, 10% glycerol, and 0.03% *n*-dodecyl β-D-maltoside) and concentrated to 11 mg of Chl/mL using Microcon-100 (Amicon). Note that the Sr^{2+} ion in the OEC of Sr^{2+}−PSII of *T. elongatus* is not replaced with Ca^{2+} even in a buffer containing Ca^{2+} (*15*). Also note that a high concentration of betaine is effective to keep the O_2-evolving activity of Sr^{2+}−PSII (*15*).

The oxygen-evolving PSII membranes of spinach (*51*) were prepared as reported previously (*52*) and suspended in a pH 6.5 buffer (40 mM Mes−NaOH, 400 mM sucrose, and 20 mM NaCl). To replace Ca^{2+} with Sr^{2+} in this membrane preparation, Ca^{2+} was first depleted by the low-pH treatment (*53*, *54*). The sample was treated with a pH 3.0 citrate buffer (10 mM citrate, 400 mM sucrose, and 20 mM NaCl) for 5 min, and then 0.1 volume of pH 7.5 Mops buffer (0.5 M Mops, 400 mM sucrose, and 20 mM NaCl) was added, followed by incubation for 20 min on ice. Note that the Ca^{2+}-depleted PSII prepared by this procedure mostly retains the 24 and 16 kDa extrinsic proteins. The Ca^{2+}-depleted PSII membranes were washed with a pH 6.5 Mes buffer (buffer B: 40 mM Mes, 400 mM sucrose, 20 mM NaCl, and 0.5 mM EDTA), and then $SrCl_2$ was added to the suspension (final $SrCl_2$ concentration: 20 mM) followed by incubation for more than 1 h on ice. The control Ca^{2+}−PSII sample was prepared by addition of 20 mM $CaCl_2$ instead of $SrCl_2$ at the last step. The Ca^{2+}-reconstituted sample recovered about 66% of the O_2-evolving activity of untreated PSII membranes [660 μM O_2/(mg of Chl h)]. The activity of Sr^{2+}-substituted PSII membranes was ~58% of that of the Ca^{2+}-reconstituted PSII, which is comparable to the decrease in O_2-evolving activity by a factor of 2.2−2.4 by Ca^{2+}/Sr^{2+} exchange in the PSII core complexes of *T. elongatus* (*15*).

[2] Although the authors of ref *49* claimed that the PSII preparation that they used underwent the full S-state cycle, the reported FTIR difference spectra (Figure 2 of ref *49*) showed an almost flat feature in the symmetric COO^- region (1450−1300 cm^{-1}) at the third and fourth flashes. This *clearly* indicates that the S-state transitions were blocked after the S_3 state. This flat spectral feature at the third and fourth flashes was very similar to that in the previous study by the same group (*48*) using the PSII preparation limited in water content, in which the S_3-to-S_0 transition was blocked. The fact that each flash produces a similar amount of reduced ferrocyanide does not imply that the electron comes from the Mn cluster. Readers can compare the FTIR difference spectra of the S-state cycle in ref *49* with those of our group (Figure 1 in the present study; *26*, *27*, *30*, *39*) and also of other two groups (*25*, *32*−*35*, *37*). The S-state spectra of the latter three groups are basically in agreement with each other and show clear bands in the 1450−1300 cm^{-1} region at the third and fourth flashes.

For FTIR measurements, samples were loaded between a pair of CaF_2 plates (25 mm in diameter) as described previously (*26*). For the PSII core complexes of *T. elongatus*, when ferricyanide is used as an exogenous electron acceptor, 2 μL of 100 mM potassium ferricyanide was first dried at the center of the CaF_2 plate and then was mixed with 2 μL of the PSII core suspension in buffer A (11 mg of Chl/mL). This solution sample was covered with another CaF_2 plate and sealed with silicone grease. A piece of aluminum foil ($\sim$1 mm $\times$ $\sim$1 mm; $\sim$15 μm in thickness) was placed as a spacer in the outer part of the IR cell. When PpBQ was used as an electron acceptor, 0.5 μL of 500 mM PpBQ/DMSO was mixed with 10 μL of the *T. elongatus* core suspension (final PpBQ concentration: 25 mM), and 2 μL of this mixture was sandwiched between the CaF_2 plates in a similar manner. In contrast to the previous studies in which hydration films of the core complexes were used (*27*, *30*, *39*), solution samples were preferred in this study, because they included a high concentration of betaine and partial drying of the sample would increase too much the betaine concentration. For the PSII membranes from spinach, 1 mL of the sample suspension (0.5 mg of Chl/mL) in buffer B in the presence of 20 mM $CaCl_2$ or $SrCl_2$ was mixed with 10 μL of 500 mM PpBQ/DMSO (final PpBQ concentration: 5 mM) and was centrifuged at 174000*g* for 45 min. The resultant pellet was sandwiched between CaF_2 (for Ca^{2+}−PSII) or ZnSe (for Sr^{2+}−PSII) plates and sealed with silicone grease. An aluminum foil spacer was not necessary to keep the thickness of this pellet sample.

FTIR spectra were recorded using a Bruker IFS-66/S spectrophotometer equipped with an MCT detector (InfraRed D316/8) (*26*, *27*). The sample temperature was adjusted to 10 °C by circulating cold water in a copper holder. Flash illumination was performed using a Q-switched Nd:YAG laser (Quanta-Ray GCR-130; wavelength, 532 nm; pulse width, $\sim$7 ns fwhm; intensity, $\sim$7 mJ pulse^{-1} cm^{-2} at the sample surface). After two preflashes (1 Hz) and subsequent dark relaxation for a certain period (see below), four consecutive flashes were applied to the sample with 20 s intervals for *T. elongatus* core complexes and 4 s intervals for spinach PSII membranes. Single-beam spectra (acquisition mode: double-sided fast return) with 40 scans (20 s accumulation) and 8 scans (4 s accumulation) for *T. elongatus* and spinach, respectively, were recorded before, between, and after the flashes. A longer accumulation time was adopted for the *T. elongatus* core sample because of the slower relaxation rates of the S_2 and S_3 states in comparison with the spinach sample (see below). Before the first flash, two single-beam spectra were recorded to calculate the noise level. After dark relaxation (see below), the entire cycle was repeated, and the spectra of 2, 4, and 12 cycles for the *T. elongatus* core complexes with ferricyanide, those with PpBQ, and spinach PSII membranes, respectively, were averaged for one sample. The fewer repetition cycles for the *T. elongatus* core with ferricyanide were to avoid the contamination of the Y_D signal due to the increase in ferrocyanide concentration. Difference spectra upon individual flashes (after-minus-before the flash) and a dark-minus-dark difference spectrum before the train of flashes were calculated using the obtained single-beam spectra. The spectra of several samples were averaged to improve the signal-to-noise ratios. The dark relaxation periods after the preflashes and between the cycles were 60 and 90 min for Ca^{2+}− and Sr^{2+}−PSII, respectively, of *T. elontgatus* with ferricyanide, 100 and 120 min for Ca^{2+}− and Sr^{2+}−PSII, respectively, of *T. elontgatus* with PpBQ, and 30 min for both Ca^{2+}− and Sr^{2+}−PSII of spinach. These dark periods were determined from the relaxation time of the S_3/S_2 states estimated as described previously (*27*). Note that much longer dark periods were necessary for the *T. elongatus* core complexes in the present study in comparison with the previous solution sample (10 min) (*26*), probably because of the presence of 1 M betaine and 10% glycerol in the samples. The spectral resolution was 4 cm^{-1}.

To study the flash-number dependence of signal intensities, FTIR spectra were recorded basically under the same conditions except that 12 consecutive flashes were applied to the sample. In addition, for the PSII membrane preparation, a spectral resolution of 16 cm^{-1} was used to obtain a better signal-to-noise ratio. The total number of flashes subjected to one sample was adjusted to that of the above four-flash measurements as much as possible by changing the repetition number of the cycle. Several samples were used to average the data.

RESULTS

Figure 1 shows flash-induced FTIR spectra of the S-state cycle of the PSII core complexes of *T. elongatus* in the presence of ferricyanide (blue lines) and PpBQ (red lines) as exogenous electron acceptors and the PSII membranes of spinach in the presence of PpBQ (green lines). All of these samples include Ca^{2+} in the OEC. Although the Ca^{2+}-containing PSII sample from spinach was prepared by adding Ca^{2+} to Ca^{2+}-depleted PSII membranes (by low-pH treatment), as a control sample for Sr^{2+}-reconstituted PSII, the obtained spectra were basically identical to the native PSII membranes (not shown) except for relatively large non-heme iron signals (see below) due to partial inactivation of OEC during Ca^{2+} depletion. Measurements of the spinach PSII membranes were also performed using other electron acceptors, i.e., ferricyanide, 2,5-DCBQ, and duroquinone, but the results showed less efficient S-state cycling compared with the measurement using PpBQ. Because the present study focused on the carboxylate stretching vibrations in the regions of 1600−1300 cm^{-1}, a relatively large amount of sample was loaded so that the absorbance of the $\sim$1650 cm^{-1} peak due to the amide I and water bands exceeds 1.0. This condition significantly enhanced the noise level of the region of 1700−1610 cm^{-1}, and hence we did not present spectra in this region in Figure 1.

The first- (a), second- (b), third- (c), and fourth- (d) flash spectra represent the structural changes of the $S_1 \rightarrow S_2$, $S_2 \rightarrow S_3$, $S_3 \rightarrow S_0$, and $S_0 \rightarrow S_1$ transitions, respectively (*25*, *26*). Previous studies of isotope substitution showed that basically all of the bands at 1450−1300 cm^{-1} arise from the symmetric COO^- stretching vibrations of carboxylate groups and those at 1600−1450 cm^{-1} arise from the asymmetric COO^- stretching and the amide II (NH bend plus CN stretch) vibrations (*30*). The spectra of *T. elongatus* using ferricyanide and PpBQ as electron acceptors showed basically identical band features, indicating that the contribution of PpBQ bands is negligible in the presented region. The absence of a positive peak around 1480 cm^{-1} due to

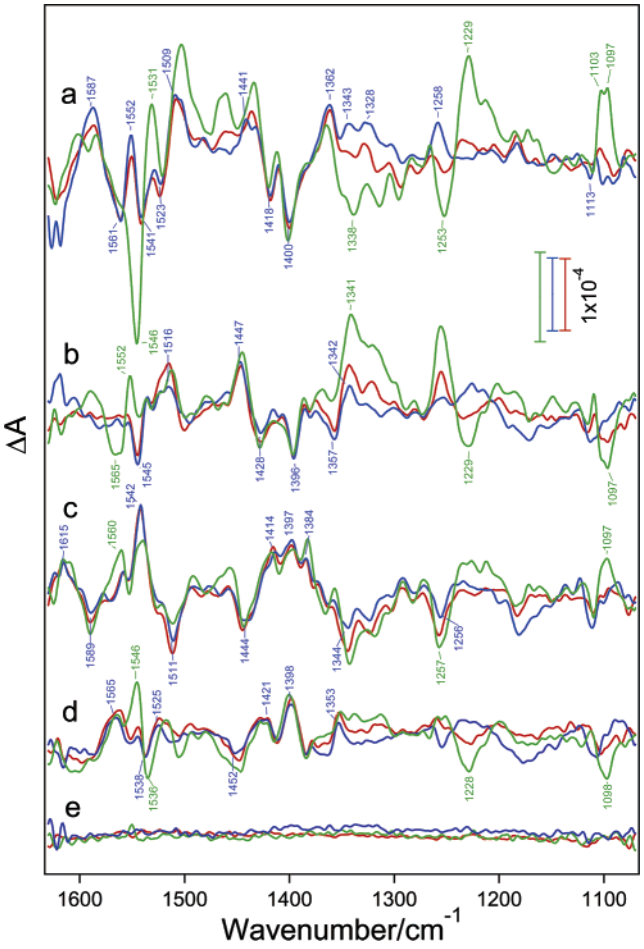

FIGURE 1: Flash-induced FTIR difference spectra of OEC during the S-state cycle measured using the Ca^{2+}−PSII core complexes of *T. elongatus* in the presence of ferricyanide (blue lines) and PpBQ (red lines) and using the Ca^{2+}-reconstituted PSII membranes of spinach in the presence of PpBQ (green lines). The difference spectra were recorded upon the first- (a), second- (b), third- (c), and fourth- (d) flash illumination, representing the $S_1 \rightarrow S_2$, $S_2 \rightarrow S_3$, $S_3 \rightarrow S_0$, and $S_0 \rightarrow S_1$ transitions, respectively. The dark-minus-dark difference spectra (e) recorded before the train of flashes express the noise levels. The scale bars in blue, red, and green colors represent the scales ($\Delta A = 1 \times 10^{-4}$) of the corresponding spectra in the same colors. The single-beam spectra with 360, 320, and 480 scans in total were averaged for the *T. elongatus* complexes with ferricyanide, those with PpBQ, and the spinach membranes with PpBQ, respectively.

the semiquionone CO vibration in the spectra with PpBQ (Figure 1, red lines) indicates that PpBQ was converted to the quinol form ($PpBQH_2$) upon reduction either by the reaction with the non-heme iron (see below) or by disproportionation. From a multiflash experiment, the intensities of $PpBQH_2$/PpBQ difference signals in the 1600−1300 cm^{-1} region per a single flash were estimated to be smaller than 10^{-5}. The spectra of Ca^{2+}-reconstituted PSII membranes of spinach were also very similar to those of *T. elongatus* in the 1500−1340 cm^{-1} region. However, spectral features in the regions of 1600−1500 and 1340−1090 cm^{-1} were rather different from those of *T. elongatus*. In the first-flash spectrum, prominent peaks were observed at 1097, 1103, 1229, 1253, 1338, and 1546 cm^{-1}. These peaks arise from the non-heme iron on the electron acceptor side (*55*, *56*), which was oxidized from Fe^{2+} to Fe^{3+} by singly photoreduced PpBQ (*57*, *58*). The peaks around 1100 cm^{-1} and in 1340−1220 cm^{-1} have been assigned to the histidine and bicarbonate, respectively, ligated to the non-heme iron (*55*), and the peak near 1546 [at 1552 cm^{-1} in the original Fe^{3+}/Fe^{2+} spectrum (*55*, *56*)] is probably due to the amide II band. These peaks clearly showed a period 2 oscillation by subsequent flashes in agreement with the previous observation using EPR spectroscopy (*57*, *58*), supporting the above assignment to the non-heme iron signals. It is noted that the spectra of *T. elongatus* using PpBQ as an exogenous electron acceptor (red lines) showed similar features in the non-heme iron region, although their intensities were much smaller. This indicates that Fe oxidation by reduced PpBQ also takes place in the core complexes of *T. elongatus*, but in fewer centers. Fortunately, the non-heme iron spectrum does not exhibit prominent features in most of the symmetric COO^- stretching region (1450−1300 cm^{-1}), and thus the effect of Ca^{2+}/Sr^{2+} exchange in spinach PSII membranes on this region can be analyzed without the interference of the non-heme iron signals.

Figure 2 shows the flash-induced FTIR spectra of the S-state cycle of the biosynthetically Sr^{2+}-substituted PSII complexes of *T. elongatus* (red lines) in the presence of ferricyanide in comparison with those of Ca^{2+}−PSII complexes (blue lines). Several spectral changes were clearly observed upon Sr^{2+} substitution. In the first-flash spectra (a), the intensities of the bands of Ca^{2+}−PSII at 1362 and 1418 cm^{-1} decreased, and in the second-flash spectra (b), the peaks at 1516 and 1447 cm^{-1} were shifted to the lower frequencies. At the third flash (c), the band intensity around 1365 cm^{-1} increased, and at the fourth flash (d), the 1452 cm^{-1} band was downshifted. Basically the same changes were observed for the spectra recorded using PpBQ as an electron acceptor (Figure 3).

In Figure 4, the S-state spectra of the Sr^{2+}-reconstituted PSII membranes (red lines) were compared with those of the Ca^{2+}-reconstituted sample (blue lines) in the presence of PpBQ as an electron acceptor. Spectral intensities, when normalized at the first flash, seem to be slightly smaller in Sr^{2+}−PSII at the second, third, and fourth flashes. However, the tendency of the Sr^{2+}-induced changes was very similar to the cases of *T. elongatus*, i.e., decrease in the intensities of the 1364 and 1419 cm^{-1} bands at the first flash (a), downshifts of 1512 and 1445 cm^{-1} peaks at the second flash (b), and intensity increase around 1365 cm^{-1} at the third flash (c), although the spectral change at the fourth flash was not very clear in the raw spectra (d).

The negative peak at ∼1400 cm^{-1} typical of the first-flash S_2/S_1 spectra only slightly (∼1 cm^{-1}) shifted to the higher frequency upon Sr^{2+} substitution but did not show intensity changes in all three sets of spectra (Figures 2−4, panel a). Hence, the efficiency of the S-state cycle in both Ca^{2+}− and Sr^{2+}−PSII was estimated by plotting the intensity at the frequency of this peak as a function of the flash number. Figure 5 shows the oscillation patterns of the intensities at 1400 or 1401 cm^{-1} of Ca^{2+}−PSII (blue circles) and Sr^{2+}−PSII (red circles) of *T. elongatus* with ferricyanide (A) and PpBQ (B) and those of spinach with PpBQ (C). Filled circles with solid lines and open circles with dotted lines express the experimental data and the results of simulations, respectively. Typical period 4 oscillation patterns were clearly observed in all of the samples. The S-state cycle of Sr^{2+}−PSII was as efficient as that of Ca^{2+}−PSII in *T. elongatus*, while in spinach PSII membranes, Sr^{2+}−PSII showed a

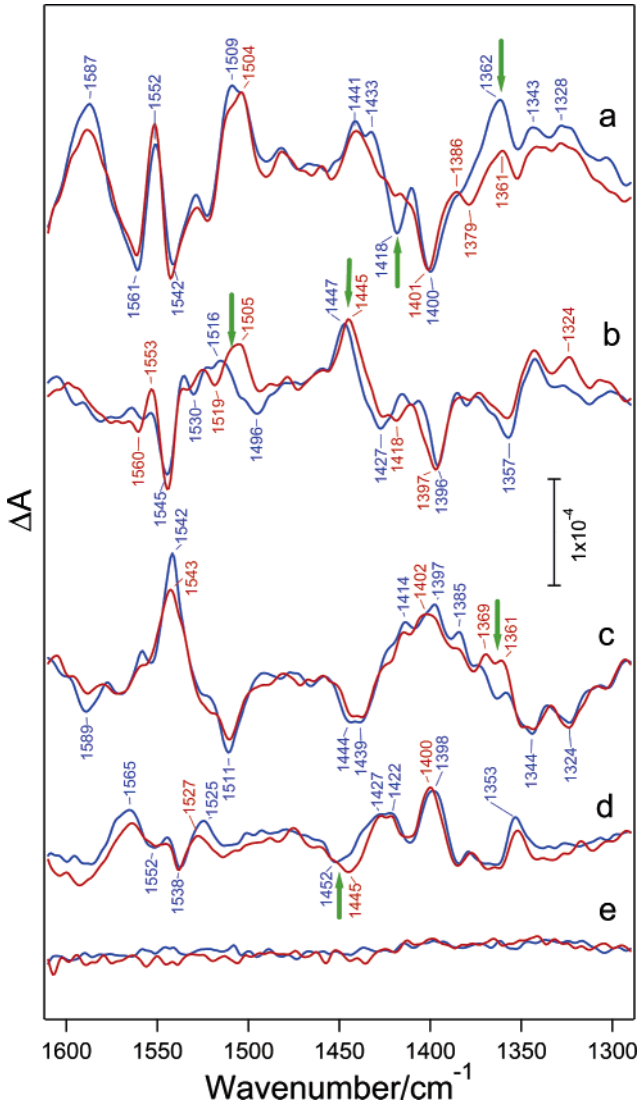

FIGURE 2: FTIR difference spectra (COO^- stretching region) of the S-state cycle of Ca^{2+}−PSII (blue lines) and Sr^{2+}−PSII (red lines) of *T. elongatus* in the presence of ferricyanide as an electron acceptor. The difference spectra were recorded upon the first- (a), second- (b), third- (c), and fourth- (d) flash illumination, representing the $S_1 \rightarrow S_2$, $S_2 \rightarrow S_3$, $S_3 \rightarrow S_0$, and $S_0 \rightarrow S_1$ transitions, respectively. The dark-minus-dark spectra (e) show the noise levels. The single-beam spectra with 360 and 400 scans in total were averaged for Ca^{2+}− and Sr^{2+}−PSII, respectively. Green arrows indicate the bands sensitive to Sr^{2+} substitution.

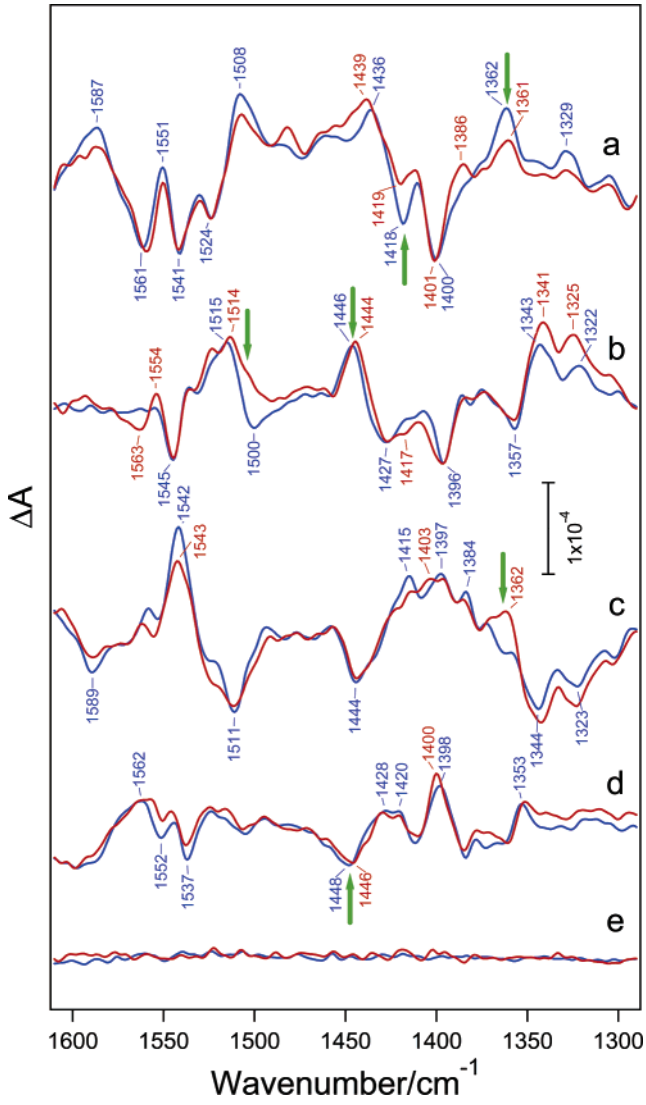

FIGURE 3: FTIR difference spectra (COO^- stretching region) of the S-state cycle of Ca^{2+}−PSII (blue lines) and Sr^{2+}−PSII (red lines) of *T. elongatus* in the presence of PpBQ as an electron acceptor. The difference spectra were recorded upon the first- (a), second- (b), third- (c), and fourth- (d) flash illumination, representing the $S_1 \rightarrow S_2$, $S_2 \rightarrow S_3$, $S_3 \rightarrow S_0$, and $S_0 \rightarrow S_1$ transitions, respectively. The dark-minus-dark spectra (e) show the noise levels. The single-beam spectra with 320 scans in total were averaged for both Ca^{2+}− and Sr^{2+}−PSII. Green arrows indicate the bands sensitive to Sr^{2+} substitution.

slightly faster damping of oscillation than Ca^{2+}−PSII. In fact, by the simulations, the miss factors were estimated to be 0.05 and 0.09 for Ca^{2+}−PSII and Sr^{2+}−PSII, respectively, of *T. elongatus* with ferricyanide (Figure 5A), 0.11 for both Ca^{2+}−PSII and Sr^{2+}−PSII of *T. elongatus* with PpBQ (Figure 5B), and 0.07 and 0.13 for Ca^{2+}−PSII and Sr^{2+}−PSII, respectively, of spinach (Figure 5C). The efficient S-state cycle of the Sr^{2+}-substituted PSII core complexes of *T. elongatus* is consistent with the previous measurements of UV absorption changes at 292 nm (*15*). In addition, the slightly larger miss factor in the Sr^{2+}-reconstituted PSII membranes of spinach than in the corresponding Ca^{2+}−PSII preparation is in agreement with the data of mass spectrometric measurements (*23*). It should be noted that the oscillation pattern of Sr^{2+}−PSII of *T. elongatus* was slightly shifted from that of Ca^{2+}−PSII when ferricyanide was used as an electron acceptor (Figure 5A). This could be caused by Y_D to $Y_D^{\bullet}$ oxidation at the first flash in some centers of Sr^{2+}−PSII in the presence of ferricyanide/ferrocyanide. This is also suggested by the presence of a small negative peak at 1704 cm^{-1} typical of the $Y_D^{\bullet}/Y_D$ signal (*59*) in the first-flash spectrum of this sample (not shown). Such a contribution of the $Y_D^{\bullet}$ signal, however, was not observed when PpBQ was used as an electron acceptor for both the *T. elongatus* and spinach samples.

The effects of Sr^{2+} substitution can be more clearly shown by calculating Ca^{2+}-minus-Sr^{2+} double difference spectra. Figure 6 shows the double difference spectra of *T. elongatus* core complexes with ferricyanide (blue lines) and PpBQ (red lines) and of spinach PSII membranes (green lines) at the first (a), second (b), third (c), and fourth (d) flashes with a noise level as a double difference of dark-minus-dark spectra (e). For the *T. elongatus* core complexes, the same subtraction factors were used for all of the four flash-induced

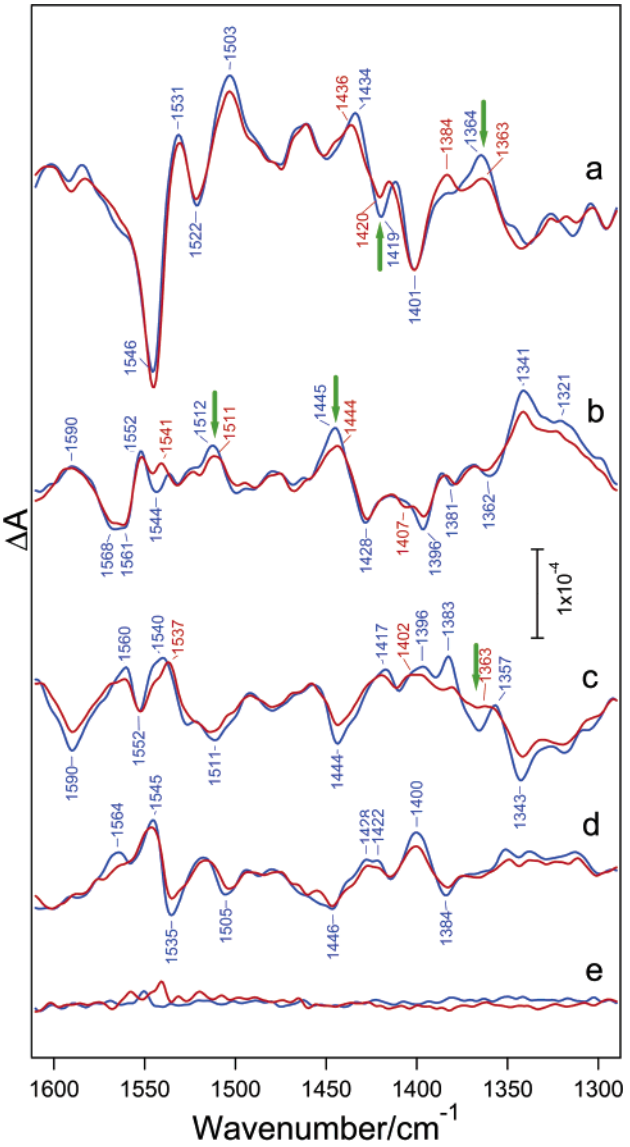

FIGURE 4: FTIR difference spectra (COO^- stretching region) of the S-state cycle of the Ca^{2+}- (blue lines) and Sr^{2+}- (red lines) reconstituted PSII membranes of spinach in the presence of PpBQ as an electron acceptor. The difference spectra were recorded upon the first- (a), second- (b), third- (c), and fourth- (d) flash illumination, representing the $S_1 \rightarrow S_2$, $S_2 \rightarrow S_3$, $S_3 \rightarrow S_0$, and $S_0 \rightarrow S_1$ transitions, respectively. The dark-minus-dark spectra (e) show the noise levels. The single-beam spectra with 480 scans in total were averaged for both Ca^{2+}− and Sr^{2+}−PSII. Green arrows indicate the bands sensitive to Sr^{2+} substitution.

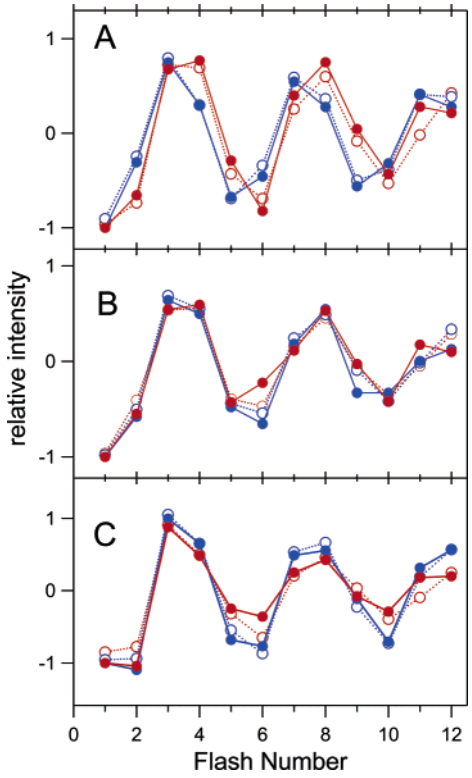

FIGURE 5: Flash-number dependence of the relative intensities of the COO^- bands at ~1400 cm^{-1} of Ca^{2+}−PSII (blue circles with blue lines) and Sr^{2+}−PSII (red circles with red lines). The experimental data are expressed by filled circles with solid lines, and the results of simulations are shown in open circles with dotted lines. (A) PSII core complexes of *T. elongatus* in the presence ferricyanide. (B) PSII core complexes of *T. elongatus* in the presence of PpBQ. (C) PSII membranes of spinach in the presence of PpBQ. The intensities of the 1400 or 1401 cm^{-1} peak in the first-flash spectra were normalized to −1, and the relative intensities at the same frequencies in the *n*th-flash spectra ($n > 1$) were plotted.

spectra, while for the PSII membranes of spinach, subtraction factors were changed for individual spectra because of the slightly higher miss factor in Sr^{2+}−PSII compared with Ca^{2+}−PSII.

The double difference spectra of the three sets of samples were all very similar at each flash, despite the differences in electron acceptors (ferricyanide and PpBQ), the species (*T. elongatus* and spinach), and preparations (PSII core complexes and PSII-enriched membranes). In particular, the band features and peak positions in the symmetric COO^- stretching region (1450−1350 cm^{-1}) were mostly identical between the three, indicating that the slight difference in the miss factor between Ca^{2+}−PSII and Sr^{2+}−PSII of the spinach membranes did not affect the double difference spectra. Also, the spectra in the asymmetric COO^- region (1600−1500 cm^{-1}) of *T. elongatus* with different electron acceptors were mostly the same, except for the features around 1550 cm^{-1} at the first flash. Thus, the contributions of the acceptor side signals (e.g., quinones, non-heme iron) were negligible in the present double difference spectra. The slight difference in the first-flash spectra could be due to the $Y_D^{\bullet}/Y_D$ contamination in the Sr^{2+}−PSII spectra.

The feature of the symmetric COO^- region at the first flash ($S_1 \rightarrow S_2$ transition) was mostly identical to the corresponding Ca^{2+}-minus-Sr^{2+} spectra reported previously for the *Synechocystis* core complexes (*47*) and the spinach core or membrane samples (*46*, *48*, *49*); the peaks at 1446(−)/1432−1(+)/1418(−)/1409−3(+)/1395−84(−)/1365−3(+) cm^{-1} in the present study (Figure 6a) correspond to those at 1447(−)/1433−2(+)/1419−7(−)/1409−8(+)/1395−87(−)/1365−3(+) cm^{-1} in the previous studies. Also, the features in the asymmetric COO^- and amide II regions in the first-flash spectrum of the *T. elongatus* core complexes with PpBQ [1586(+)/1567(−)/1555(+)/1540(−)/1532(+)/1520(−) cm^{-1}; Figure 6a, red line] were similar to those of the *Synechocystis* core complexes [1585(+)/1564(−)/1551(+)/1543(−)/1533(+)/1519(−) cm^{-1} (*47*)], and the peaks in this region of spinach PSII membranes at 1587(+)/1567(−)/1541(+)/1508(+) cm^{-1} (Figure 6a, green line) may correspond to the peaks at 1587(+)/1570(−)/1539(+)/1504(+) cm^{-1} in the previous spectra of spinach membranes (*48*). Note that, in the previous studies, the PSII core (*46*) and

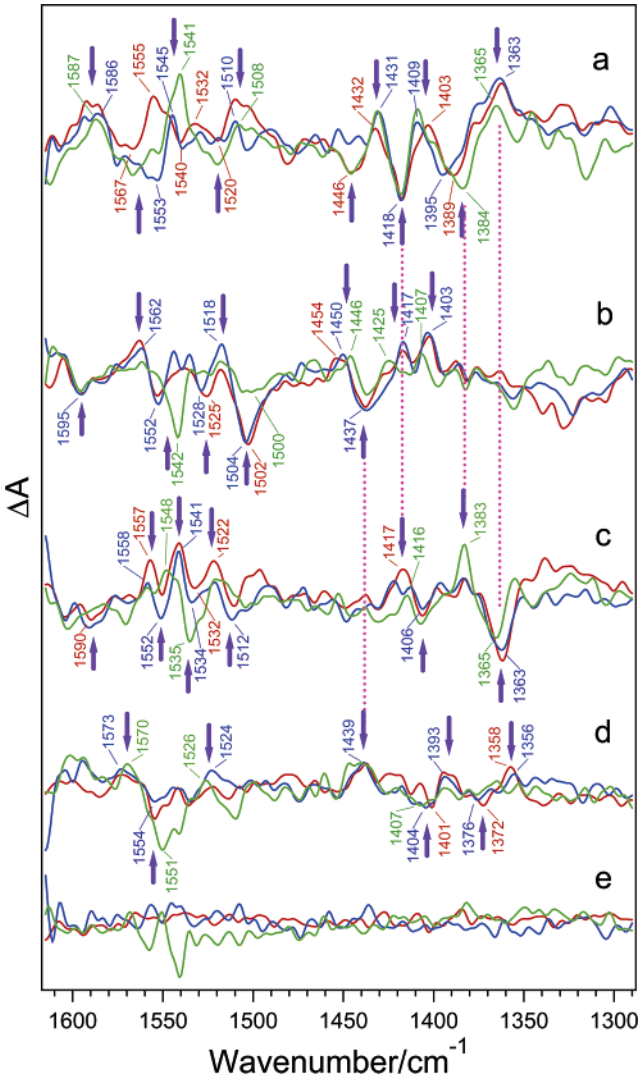

FIGURE 6: Ca^{2+}-minus-Sr^{2+} double difference spectra of the S-state cycle of the PSII core complexes of *T. elongatus* in the presence of ferricyanide (blue lines) and PpBQ (red lines) and of the PSII membranes of spinach in the presence of PpBQ (green lines). The double difference spectra at the first- (a), second- (b), third- (c), and fourth- (d) flash illumination, representing the $S_1 \rightarrow S_2$, $S_2 \rightarrow S_3$, $S_3 \rightarrow S_0$, and $S_0 \rightarrow S_1$ transitions, respectively, and the nose level (e) were calculated from the corresponding flash-induced and dark-minus-dark difference spectra in Figures 2−4. Subtraction factors were determined so as to delete the spectral features as much as possible. For the *T. elongatus* samples, the same subtraction factors were used throughout the first- to fourth-flash spectra. For the PSII membranes of spinach, different subtraction factors were used for individual flash-induced spectra, because the miss factor in Sr^{2+}−PSII was slightly higher than that in Ca^{2+}−PSII (Figure 5). Purple arrows indicate the bands commonly observed in the three spectra.

membrane (*48*) preparations are depleted of 23 and 16 kDa extrinsic proteins by salt wash, whereas our sample basically includes these proteins. Hence, this similarity of the Ca^{2+}-minus-Sr^{2+} double difference spectra for the $S_1 \rightarrow S_2$ transition indicates that the 23 and 16 kDa proteins do not affect the structural changes of the Mn cluster upon Ca^{2+}/Sr^{2+} exchange.

In contrast to the close similarity of all the double difference spectra in the symmetric COO^- region (Figure 6), some differences were seen around 1550 cm^{-1} in the asymmetric COO^- and amide II region between the spinach (Figure 6, green lines) and *T. elongatus* (Figure 6, blue and red lines) samples. For example, the peaks at 1541(+), 1542(−), and 1548(+) cm^{-1} in the first-, second-, and third-flash spectra of spinach (Figure 6, green lines), respectively, showed shifted frequencies, and the peaks at 1535(−) and 1551(−) cm^{-1} at the third and fourth flashes, respectively, exhibited much stronger intensities. Because of the close similarity in the symmetric COO^- region, these differences could be ascribed to the amide II vibrations of backbone amides, which can be changed by different species, rather than the asymmetric COO^- vibrations coupled to the symmetric ones. Note that the non-heme iron signals that have a large contribution to the S-state spectra of spinach (Figure 5) are not responsible for the difference in this region, because in the double difference spectra, no specific peaks were observed at 1338, 1257, 1228, 1103, and 1097 cm^{-1} (not shown) where typical non-heme iron signals exist (Figure 1) (*55*, *56*). Taking into consideration the comparable numbers of peaks in the symmetric and asymmetric COO^- regions, it is surmised that the peaks in 1600−1500 cm^{-1} commonly observed in both species arise from the asymmetric COO^- vibrations.

Depending on the flash number, characteristic band features were observed in the double difference spectra. At the first flash (Figure 6a), several prominent peaks were observed in both the asymmetric and symmetric COO^- regions, i.e., peaks at ∼1587(+)/∼1567(−)/1555−41(+)/∼1520(−)/1510−08(+) cm^{-1} and at 1446(−)/1432−1(+)/1418(−)/1409−3(+)/1395−84(−)/1365−3(+) cm^{-1}. At the second flash (Figure 6b), the prominent common features are the relatively strong peaks at 1504−1500(−) and 1437(−) cm^{-1} with satellite peaks at 1518(+) and 1454−46(+) cm^{-1}. Other medium peaks are observed at 1595(−)/1562(+)/1552−42(−)/1528−5(+) cm^{-1} and 1425−17(+)/1407−3(+) cm^{-1}. At the third flash (Figure 6c), the most prominent peak was observed at the relatively low frequency of 1365−3(−) cm^{-1} in the symmetric COO^- region, with a satellite peak at 1383(+) cm^{-1}. Other medium peaks in the symmetric COO^- region were observed at ∼1417(+)/1406(−) cm^{-1}. In the asymmetric COO^- region, medium or strong peaks were observed at 1590(−)/1558−7(+)/1552(−)/1548−1(+)/1535−2(−)/1522(+)/1512(−) cm^{-1}. At the fourth flash (Figure 6d), medium or weak peaks were observed at 1439(+)/1407−1(−)/1393(+)/1376−2(−)/1358−6(+) cm^{-1} in the symmetric COO^- region. In the asymmetric COO^- region, peaks were observed at 1573−70(+)/1554−1(−)/1526−4(−) cm^{-1}. It is worth noting that, in the double difference spectra at every flash, a common peak was not observed at ∼1113 cm^{-1} (not shown) where the His CN stretching band exists (*36*, *37*), indicating that the His ligand to the Mn cluster is not sensitive to the Ca^{2+}/Sr^{2+} exchange.

DISCUSSION

In this study, we have investigated the effect of Ca^{2+}/Sr^{2+} exchange on the ligand structure of the Mn cluster during the S-state cycle using FTIR different spectroscopy. Because Sr^{2+} has an ion radius larger than Ca^{2+} [1.13 and 0.99 Å for Sr^{2+} and Ca^{2+}, respectively (*7*)], the structure of the Mn cluster including its amino acid ligands should be perturbed by Ca^{2+}/Sr^{2+} exchange, if Ca^{2+} is indeed strongly coupled with the Mn cluster as proposed earlier by EPR and EXAFS spectroscopies (*3*, *15*) and now by X-ray crystallography (*8*, *9*). Despite such a structural perturbation, however, O_2-

evolving activity is retained in Sr^{2+}-substituted PSII, and hence, the structural relevance of Ca^{2+} to the Mn cluster in every metastable S state (S_0-S_3) can be examined by comparing the flash-induced FTIR difference spectra of the S-state cycle in Sr^{2+}−PSII with those of Ca^{2+}−PSII. In particular, such information in the S_3 and S_0 states cannot be obtained in Ca^{2+}-depleted PSII or other metal-substituted PSII because of the inhibition of the transitions beyond the S_2 state in these preparations (*1*, *6*, *7*).

The relatively small miss factors (0.05−0.13) estimated from the flash-number dependence of the FTIR signal (Figure 5) guaranteed that the first-, second-, third-, and fourth-flash spectra virtually represent the structural changes upon the $S_1 \rightarrow S_2$, $S_2 \rightarrow S_3$, $S_3 \rightarrow S_0$, and $S_0 \rightarrow S_1$ transitions, respectively. All three kinds of samples, i.e., the PSII core complexes of *T. elongatus* with ferricyanide as an electron acceptor, and those with PpBQ, and the PSII membranes of spinach with PpBQ, showed common features of Ca^{2+}-minus-Sr^{2+} double difference spectra, especially in the symmetric COO^- region (1450−1300 cm^{-1}) (Figure 6). This strongly indicates that the observed signals truly arise from the OEC but not from some other origins such as Y_D, non-heme iron, and quinones, which could contaminate the S-state spectra. In addition, these common features between the *T. elongatus* and spinach samples indicate that the relevance of Ca^{2+} to the ligand structure of the Mn cluster during the S-state cycle is basically identical between cyanobacteria and plants as proposed previously (*15*).

General correlations have been known between the coordination structures of carboxylate groups and the frequency gaps between the symmetric and asymmetric COO^- stretching vibrations ($\Delta\nu_{as-s}$) (*42*−*44*): (1) the unidentate structure shows a relatively large difference of >200 cm^{-1}; (2) the chelating bidentate structure shows a relatively small frequency gap of <100 cm^{-1}; (3) the bridging bidentate structure show a medium-frequency gap close to the ionic values (∼164 cm^{-1}). We will interpret the carboxylate bands in the difference spectra of the S-state cycle (Figures 2−4 and 6) using these correlations as criteria, bearing in mind that they are not necessarily strict (*42*, *60*).

In the first-flash spectrum ($S_1 \rightarrow S_2$ transition) of each of the three samples (Figures 2−4, panel a), the intense positive peak at 1364−2 cm^{-1} in the symmetric COO^- region significantly decreased its intensity upon Sr^{2+} substitution. This intensity decrease is probably linked to the intensity increase at the similar position in the third-flash spectra ($S_3 \rightarrow S_0$ transition) (Figures 2−4, panel c), because structural changes in the $S_1 \rightarrow S_2$ transition must be reversed in another transition. In the Ca^{2+}-minus-Sr^{2+} double difference spectra, these observations correspond to strong positive and negative peaks at 1365−3 cm^{-1} at the first (Figure 6a) and third (Figure 6c) flashes, respectively. This intensity decrease seems to be coupled with the appearance of a positive intensity at 1386−4 cm^{-1} in the first-flash spectra of Sr^{2+}-substituted PSII (Figures 2−4, panel a, red lines), which corresponds to a strong negative peak at 1395−84 cm^{-1} in the double difference spectra (Figure 6a). The counter peak at the third flash was observed at 1383 cm^{-1} with a strong intensity in the spinach sample (Figure 6c, green line) and with weaker intensities in the *T. elongatus* samples (Figure 6, blue and red lines). These band changes can be caused by the upshifts of the band at ∼1363 cm^{-1} in the S_2 and S_3 states to ∼1385 cm^{-1} upon Sr^{2+} substitution. The asymmetric COO^- region of the double difference spectra at the first and third flashes (Figure 6a,c) showed complex band features at 1590−1505 cm^{-1}, which should include the asymmetric COO^- bands coupled to the above symmetric bands. Thus, the frequency gap, $\Delta\nu_{as-s}$, can be in the range of 230−120 cm^{-1}, indicative of a bridging or unidentate coordination structure.

Another prominent effect of Sr^{2+} substitution on the first-flash spectra is a clear intensity decrease of the negative 1419−8 cm^{-1} peak concomitant with a slight shift or an intensity change of the neighboring positive peak at 1441−34 cm^{-1} (Figures 2−4, panel a). These spectral changes were expressed in the Ca^{2+}-minus-Sr^{2+} double difference spectra as a strong negative peak at 1418 cm^{-1} with negative/positive peaks at 1446/1432−1 cm^{-1} (Figure 6a). This negative peak at 1418 cm^{-1} seems to correspond to the positive peak at 1417−6 cm^{-1} at the third flash (Figure 6c), which originates from the intensity decrease of the positive band at this position in the third-flash difference spectra (Figures 2−4, panel c). The coupled asymmetric COO^- vibration may be present also in the complex features in 1590−1505 cm^{-1} of the first- and third-flash double difference spectra (Figure 6a, c), and thus the $\Delta\nu_{as-s}$ value would be at 175−85 cm^{-1}, which indicates a chelating or bridging structure. This carboxylate stays in this coordination structure at least in the S_1 and S_0 states.

In the second-flash spectra representing the $S_2 \rightarrow S_3$ transition, the positive peaks at 1447−5 and 1516−2 cm^{-1} showed clear downshifts to 1445−4 and 1514−05 cm^{-1}, respectively (Figures 2−4, panel b). These changes were expressed in the double difference spectra as strong negative peaks at 1437 and 1504−0 cm^{-1} with satellite positive peaks at 1454−46 and 1518 cm^{-1} (Figure 6b). The $\Delta\nu_{as-s}$ was ∼65 cm^{-1}, indicating a chelating structure. This strong negative peak at 1437 cm^{-1} in the symmetric COO^- region seems to correspond to the positive peak at 1439 cm^{-1} at the fourth flash (Figure 6d), although the counter peak in the asymmetric COO^- region was not clearly identified. The 1439 cm^{-1} peak originates from a downshift of the negative peak at 1452−46 cm^{-1} in the fourth-flash spectra (Figures 2−4, panel d). Thus, the chelating carboxylate ligand having a symmetric COO^- frequency of ∼1437 cm^{-1} may exist in the S_3 and S_0 states.

The above interpretation for the Ca^{2+}/Sr^{2+}-sensitive peaks can be summarized as follows. In the Mn_4Ca cluster, there are at least three carboxylate ligands whose structures are significantly perturbed by Sr^{2+} substitution. They are (1) the carboxylate ligand having a bridging or unidentate structure in the S_2 and S_3 states and perturbed in the $S_1 \rightarrow S_2$ and $S_3 \rightarrow S_0$ transitions, (2) that with a chelating or bridging structure in the S_1 and S_0 states and also perturbed in the $S_1 \rightarrow S_2$ and $S_3 \rightarrow S_0$ transitions, and (3) that with a chelating structure in the S_3 and S_0 states and changes in the $S_2 \rightarrow S_3$ and $S_0 \rightarrow S_1$ transitions. It is noted that at present the possibility cannot be excluded that the carboxylate groups assigned to the bridging ligands in the above interpretations actually have a pseudo-bridging (one oxygen atom is engaged in a hydrogen bond) or ionic structure, which shows a $\Delta\nu_{as-s}$ value similar to the bridging structure (*42*, *43*). Further careful studies using deuterated, Sr^{2+}-substituted samples are necessary to address this question.

Previously, Noguchi et al. (*28*) reported that, upon Ca^{2+} depletion, the major symmetric COO^- peaks at 1403(−)/1364(+) cm^{-1} in the S_2/S_1 difference spectra are lost concomitantly with the disappearance of the asymmetric peaks at 1560(−)/1587(+) cm^{-1}. Later, Kimura et al. (*45*, *61*), claimed in their studies using Chelex-treated buffers that Ca^{2+} depletion itself does not change the S_2/S_1 spectrum at all, but the presence of chelators and a potassium ion in a buffer induces the spectral changes. However, the results of the present study together with previous studies (*46*−*49*) showed that FTIR spectra of the S-state cycle are clearly different between Ca^{2+}−PSII and Sr^{2+}−PSII, indicating that the ligand structure of the Mn cluster is somewhat different between them, although both of the Ca^{2+}− and Sr^{2+}−PSII samples show high O_2-evolving activity. Thus, it is unreasonable that Ca^{2+}-depleted OEC, which is the same as Sr^{2+}-depleted OEC, has exactly the same structure as Ca^{2+}-bound OEC but has a different structure from Sr^{2+}-bound OEC. Also, the strong structural coupling of Ca^{2+} with the Mn cluster shown in the present study and other spectroscopies (*3*, *7*) is clearly contradictory to the idea that Ca^{2+} depletion does not induce any changes in the vibrational structures of the Mn cluster (*45*, *61*). This argument strongly suggests that the Chelex-treated PSII sample that Kimura et al. (*45*, *61*) claimed as "Ca^{2+}-depleted" PSII is actually contaminated with Ca^{2+}, and the presence of chelators or metal substitution is necessary to remove such Ca^{2+} contamination.

From the large change in $\Delta\nu_{as-s}$ of the asymmetric/symmetric COO^- bands lost by Ca^{2+} depletion from the S_1 state (1560/1403 cm^{-1}; $\Delta\nu_{as-s} = 157$ cm^{-1}) to the S_2 state (1587/1364 cm^{-1}; $\Delta\nu_{as-s} = 223$ cm^{-1}), Noguchi et al. (*28*) proposed that a certain carboxylate ligand changes its coordination structure from the bridging to unidentate coordination upon the $S_1 \rightarrow S_2$ transition. They further proposed the view that this carboxylate group bridges the Mn and Ca ions and the ligation to the Ca ion is broken upon S_2 formation. In the present study, it has been observed that the 1364−2 cm^{-1} band in the S_2 state, which may correspond to the 1364 cm^{-1} peak sensitive to Ca^{2+} depletion, is drastically changed by Sr^{2+} substitution and seems to upshift to ∼1385 cm^{-1}. The coupled asymmetric band at 1587 cm^{-1} is also affected by Sr^{2+} substitution (Figures 2−4, panel a), which was expressed as a positive feature at 1587−6 cm^{-1} in the Ca^{2+}-minus-Sr^{2+} double difference spectrum (Figure 6a). One of the speculative explanations for these observations is as follows. Upon oxidation of Mn^{3+} to Mn^{4+} in the $S_1 \rightarrow S_2$ transition, the Mn−O bond in the Mn−OCO−Ca bridge is shortened, and instead the Ca−O bond is lengthened and as a result this bond will be broken. However, when Ca^{2+} is replaced with Sr^{2+}, the larger ionic radius of Sr^{2+} [by 0.14 Å (*7*)] could retain the Sr−O bond, which causes the upshift of the symmetric stretching frequency. On the other hand, the strong negative peak at ∼1400 cm^{-1} in the S_1 state showed an only slight upshift by ∼1 cm^{-1} (Figures 2−4, panel a), which seems to contradict the assignment of this peak to the carboxylate bridge between the Mn and Ca ions. However, it is possible that the structure of the carboxylate group bridging $Mn^{3+(or\ 4+)}$ and Ca^{2+} is rather asymmetric and the C−O bond attached to Mn is longer than the other C−O bond ligating Ca, and hence the C−O bond ligating Mn mainly contributes to the lower frequency (so-called symmetric) COO^- vibration. Thus, Sr^{2+} substitution for Ca^{2+} might not significantly affect the symmetric COO^- vibration. This suggests that the absence of a large shift of the ∼1400 cm^{-1} band upon Sr^{2+} substitution does not necessarily exclude the possibility that this carboxylate group forms a bridge between Mn and Ca.

In the recent X-ray crystallographic model of the Mn_4Ca cluster at 3.0 Å resolution (*9*), the carboxylate groups of D1-Ala344 (C-terminus) and of D1-Gln189 were identified as possible ligands to Ca^{2+} forming carboxylate bridges with Mn ions. The FTIR study by Chu et al. (*31*) using L-[1-^{13}C]-alanine-labeled core complexes of *Synechocystis* sp. PCC6803 showed that the carboxylate of D1-Ala344 has a symmetric COO^- band at ∼1356 cm^{-1} in the S_1 state, which moves to ∼1337 or ∼1320 cm^{-1} in the S_2 state. Also, Kimura et al. (*34*) showed that this change is reversed upon the $S_3 \rightarrow S_0$ transition. Thus, D1-Ala344 has symmetric COO^- frequencies at ∼1356 cm^{-1} in the S_1 and S_0 states and at ∼1337 or ∼1320 cm^{-1} in the S_2 and S_3 states. Strickler et al. (*47*) further showed that these D1-Ala344 bands in the S_2/S_1 spectra were not sensitive to Sr^{2+} substitution. Being consistent with this result, the above symmetric COO^- frequencies of D1-Ala344 in the four S states disagree with the frequencies (∼1363, ∼1418, and ∼1446 cm^{-1}) of the COO^- bands that were found to be sensitive to Sr^{2+} substitution in the present study. Also, very recently, the careful study by Strickler et al. (*33*) using site-directed mutants at D1-Glu189 showed that the COO^- bands of this carboxylate group little contribute to the FTIR spectra during the S-state cycle. It is therefore concluded that both D1-Ala344 and D1-Glu189 are not responsible for the three carobxylate groups identified to be perturbed by Ca^{2+}/Sr^{2+} exchange.

The above argument indicates that if the X-ray crystallographic model is correct, the carboxylate groups whose FTIR bands were sensitive to Sr^{2+} substitution are not direct ligands to Ca^{2+} but ligands to the Mn ions, which are strongly coupled to the Ca^{2+} ion. These Mn ions might be directly connected to Ca^{2+} with μ-oxo bridges. It is also possible that Sr^{2+} substitution perturbs the whole structure of the Mn cluster and affects its ligand vibrations. Such structural perturbations of the Mn cluster were reflected by the significant change in the Mn−O−Mn vibration at 606 cm^{-1} (*41*, *46*), a slight increase in the average Mn−Mn distance detected by EXAFS (*62*), and the modified multiline signal in the EPR spectra (*14*, *15*). Since the carboxylate group showing the ∼1400 and ∼1364 cm^{-1} peaks in the S_1 and S_2 states, respectively, is assigned to neither D1-Ala344 nor D1-Glu189, the idea of the bridging ligand with a drastic coordination change upon the S_2 formation (*28*) is not consistent with the model by the X-ray structure. Also, the X-ray model represents the structure in an uncontrolled low redox state (*10*, *11*), and hence the ligand structure in the high S states could be rather different. Thus, it could be also possible that carboxylate groups other than D1-Ala344 and D1-Glu189 actually function as ligands to the Ca^{2+} ion in some stage of the S-state cycle. Further FTIR studies using site-directed mutants and selective isotope labeling and X-ray crystal structures at higher resolutions will provide a clearer view about the ligand structure of the Mn_4Ca cluster during the S-state cycle.

REFERENCES

1. Debus, R. J. (1992) The manganese and calcium ions of photosynthetic oxygen evolution, *Biochim. Biophys. Acta 1102*, 269−352.
2. Hillier, W., and Messinger, J. (2005) Mechanism of photosynthetic oxygen production, in *Photosystem II: The Light-Driven Water: Plastoquinone Oxidoreductase* (Wydrzynski, T., and Satoh, K., Eds.) pp 567−608, Springer, Dordrecht, The Netherlands.
3. Yachandra, V. K. (2005) The catalytic manganese cluster: Organization of the metal ions, in *Photosystem II: The Light-Driven Water:Plastoquinone Oxidoreductase* (Wydrzynski, T., and Satoh, K., Eds.) pp 235−260, Springer, Dordrecht, The Netherlands.
4. Debus, R. J. (2005) The catalytic manganese cluster: Protein ligation, in *Photosystem II: The Light-Driven Water:Plastoquinone Oxidoreductase* (Wydrzynski, T., and Satoh, K., Eds.) pp 261−284, Springer, Dordrecht, The Netherlands.
5. Åhrling, K. A., Pace, R. J., and Evans, M. C. W. (2005) The catalytic manganese cluster: Implications from spectroscopy, in *Photosystem II: The Light-Driven Water:Plastoquinone Oxidoreductase* (Wydrzynski, T., and Satoh, K., Eds.) pp 285−306, Springer, Dordrecht, The Netherlands.
6. Yocum, C. F. (1991) Calcium activation of photosynthetic water oxidation, *Biochim. Biophys. Acta 1059*, 1−15.
7. van Gorkom, H. J., and Yocum, C. F. (2005) The calcium and chloride cofactors, in *Photosystem II: The Light-Driven Water: Plastoquinone Oxidoreductase* (Wydrzynski, T., and Satoh, K., Eds.) pp 307−327, Springer, Dordrecht, The Netherlands.
8. Ferreira, K. N., Iverson, T. M., Maghlaoui, K., Barber, J., and Iwata, S. (2004) Architecture of the photosynthetic oxygen-evolving center, *Science 19*, 1831−1838.
9. Loll, B., Kern, J., Saenger, W., Zouni, A., and Biesiadka, J. (2005) Towards complete cofactor arrangement in the 3.0 Å resolution structure of photosystem II, *Nature 438*, 1040−1044.
10. Yano, J., Kern, J., Irrgang, K. D., Latimer, M. J., Bergmann, U., Glatzel, P., Pushkar, Y., Biesiadka, J., Loll, B., Sauer, K., Messinger, J., Zouni, A., and Yachandra, V. K. (2005) X-ray damage to the Mn4Ca complex in single crystals of photosystem II: A case study for metalloprotein crystallography, *Proc. Natl. Acad. Sci. U.S.A. 102*, 12047−12052.
11. Grabolle, M., Haumann, M., Muller, C., Liebisch, P., and Dau, H. (2006) Rapid loss of structural motifs in the manganese complex of oxygenic photosynthesis by x-ray irradiation at 10−300 K, *J. Biol. Chem. 281*, 4580−4588.
12. Vrettos, J. S., Stone, D. A., and Brudvig, G. W. (2001) Quantifying the ion selectivity of the Ca^{2+} site in photosystem II: Evidence for direct involvement of Ca^{2+} in O_2 formation, *Biochemistry 40*, 7937−7945.
13. Ghanotakis, D. F., Babcock, G. T., and Yocum, C. F. (1984) Calcium reconstitutes high rates of oxygen evolution in polypeptide depleted photosystem II preparations, *FEBS Lett. 167*, 127−130.
14. Boussac, A., and Rutherford, A. W. (1988) Nature of the inhibition of the oxygen-evolving enzyme of photosystem II induced by sodium chloride washing and reversed by the addition of Ca^{2+} or Sr^{2+}, *Biochemistry 27*, 3476−3483.
15. Boussac, A., Rappaport, F., Carrier, P., Verbavatz, J.-M., Gobin, R., Kirilovsky, D., Rutherford, A. W., and Sugiura, M. (2004) Biosynthetic Ca^{2+}/Sr^{2+} Exchange in the photosystem II oxygen-evolving enzyme of *Thermosynechococcus elongatus*, *J. Biol. Chem. 279*, 22809−22819.
16. Bakou, A., Buser, C., Dandulakis, G., Brudvig, G., and Ghanotakis, D. F. (1992) Calcium binding site(s) of photosystem II as probed by lanthanides, *Biochim. Biophys. Acta 1099*, 131−136.
17. Waggoner, C. M., Pecoraro, V., and Yocum, C. F. (1989) Monovalent cations (Na^+, K^+, Cs^+) inhibit calcium activation of photosynthetic oxygen evolution, *FEBS Lett. 244*, 237−240.
18. Ono, T., and Inoue, Y. (1989) Roles of Ca^{2+} in O_2 evolution in higher plant photosystem II: Effects of replacement of Ca^{2+} site by other cations, *Arch. Biochem. Biophys. 275*, 440−448.
19. Ono, T., Rompel, A., Mino, H., and Chiba, N. (2001) Ca^{2+} function in photosynthetic oxygen evolution studied by alkali metal cations substitution, *Biophys. J. 81*, 1831−1840.
20. Vrettos, J. S., Limburg, J., and Brudvig, G. W. (2001) Mechanism of photosynthetic water oxidation: combining biophysical studies of photosystem II with inorganic model chemistry, *Biochim. Biophys. Acta 1503*, 229−245.
21. Siegbahn, P. E. M. (2000) Theoretical models for the oxygen radical mechanism of water oxidation and of the water oxidizing complex of photosystem II, *Inorg. Chem. 39*, 2923−2935.
22. Dasgupta, J., van Willigen, R. T., and Dismukes, G. C. (2004) Consequences of structural and biophysical studies for the molecular mechanism of photosynthetic oxygen evolution: functional roles for calcium and bicarbonate, *Phys. Chem. Chem. Phys. 6*, 4793−4802.
23. Hendry, G., and Wydrzynski, T. (2003) ^{18}O isotope exchange measurements reveal that calcium is involved in the binding of one substrate-water molecule to the oxygen-evolving complex in photosystem II, *Biochemistry 42*, 6209−6217.
24. Noguchi, T., and Berthomieu, C. (2005) Molecular analysis by vibrational spectroscopy, in *Photosystem II: The Light-Driven Water:Plastoquinone Oxidoreductase* (Wydrzynski, T., and Satoh, K., Eds.) pp 367−387, Springer, Dordrecht, The Netherlands.
25. Hillier, W., and Babcock, G. T. (2001) S-state dependent Fourier transform infrared difference spectra for the photosystem II oxygen evolving complex, *Biochemistry 40*, 1503−1509.
26. Noguchi, T., and Sugiura, M. (2001) Flash-induced Fourier transform infrared detection of the structural changes during the S-state cycle of the oxygen-evolving complex in photosystem II, *Biochemistry 40*, 1497−1502.
27. Noguchi, T., and Sugiura, M. (2002) Flash-induced FTIR difference spectra of the water oxidizing complex in moderately hydrated photosystem II core films: Effect of hydration extent on S-state transitions, *Biochemistry 41*, 2322−2330.
28. Noguchi, T., Ono, T., and Inoue, Y. (1995) Direct detection of a carboxylate bridge between Mn and Ca^{2+} in the photosynthetic oxygen-evolving center by means of Fourier transform infrared spectroscopy, *Biochim. Biophys. Acta 1228*, 189−200.
29. Noguchi, T., Ono, T., and Inoue, Y. (1995) A carboxylate ligand interacting with water in the oxygen-evolving center of photosystem II as revealed by Fourier transform infrared spectroscopy, *Biochim. Biophys. Acta 1232*, 59−66.
30. Noguchi, T., and Sugiura, M. (2003) Analysis of flash-induced FTIR difference spectra of the S-state cycle in the photosynthetic water-oxidizing complex by uniform ^{15}N and ^{13}C isotope labeling, *Biochemistry 42*, 6035−6042.
31. Chu, H. A., Hillier, W., and Debus, R. J. (2004) Evidence that the C-terminus of the D1 polypeptide of photosystem II is ligated to the manganese ion that undergoes oxidation during the S_1 to S_2 transition: An isotope-edited FTIR study, *Biochemistry 43*, 3152−3166.
32. Debus, R. J., Strickler, M. A., Walker, L. M., and Hillier, W. (2005) No evidence from FTIR difference spectroscopy that aspartate-170 of the D1 polypeptide ligates a manganese ion that undergoes oxidation during the S_0 to S_1, S_1 to S_2, or S_2 to S_3 transitions in photosystem II, *Biochemistry 44*, 1367−1374.
33. Strickler, M. A., Hillier, W., and Debus, R. J. (2006) No evidence from FTIR difference spectroscopy that glutamate-189 of the D1 polypeptide ligates a manganese ion that undergoes oxidation during the S_0 to S_1, S_1 to S_2, or S_2 to S_3 transitions in photosystem II, *Biochemistry 45*, 8801−8811.
34. Kimura, Y., Mizusawa, N., Yamanari, T., Ishii, A., and Ono, T. (2005) Structural changes of D1 C-terminal α-carboxylate during S-state cycling in photosynthetic oxygen evolution, *J. Biol. Chem. 280*, 2078−2083.
35. Kimura, Y., Mizusawa, N., Ishii, A., Nakazawa, S., and Ono, T. (2005) Changes in structural and functional properties of oxygen-evolving complex induced by replacement of D1-glutamate 189 with glutamine in photosystem II—Ligation of glutamate 189 carboxylate to the manganese cluster, *J. Biol. Chem. 280*, 37895−37900.
36. Noguchi, T., Inoue, Y., and Tang, X.-S. (1999) Structure of a histidine ligand in the photosynthetic oxygen-evolving complex as studied by light-induced Fourier transform infrared difference spectroscopy, *Biochemistry 38*, 10187−10195.
37. Kimura, Y., Mizusawa, N., Ishii, A., and Ono, T. (2005) FTIR detection of structural changes in a histidine ligand during S-state cycling of photosynthetic oxygen-evolving complex, *Biochemistry 44*, 16072−16078.
38. Noguchi, T., and Sugiura, M. (2000) Structure of an active water molecule in the water-oxidizing complex of photosystem II as studied by FTIR spectroscopy, *Biochemistry 39*, 10943−10949.
39. Noguchi, T., and Sugiura, M. (2002) FTIR detection of water reactions during the flash-induced S-state cycle of the photosynthetic water-oxidizing complex, *Biochemistry 41*, 15706−15712.

40. Chu, H.-A., Gardner, M. T., O'Brien, J. P., and Babcock, G. T. (1999) Low-frequency Fourier transform infrared spectroscopy of the oxygen-evolving and quinone acceptor complexes in photosystem II, *Biochemistry 38*, 4533−4541.
41. Chu, H.-A., Sackett, H., and Babcock, G. T. (2000) Identification of a Mn-O-Mn cluster vibrational mode of the oxygen-evolving complex in photosystem II by low-frequency FTIR spectroscopy, *Biochemistry 39*, 14371−14376.
42. Deacon, G. B., and Phillips, R. J. (1980) Relationships between the carbon-oxygen stretching frequencies of carboxylato complexes and the type of carboxylate coordination, *Coord. Chem. Rev. 33*, 227−250.
43. Nakamoto, K. (1997) *Infrared and Raman Spectra of Inorganic and Coordination Compounds*, 5th ed., Part B, pp 59−62, John Wiley & Sons, New York.
44. Nara, M., Torii, H., and Tasumi, M. (1996) Correlation between the vibrational frequencies of the carboxylate group and the types of its coordination to a metal ion: An ab initio molecular orbital study, *J. Phys. Chem. 100*, 19812−19817.
45. Kimura, Y., Hasegawa, K., and Ono, T. (2002) Characteristic changes of the S_2/S_1 difference FTIR spectrum induced by Ca^{2+} depletion and metal cation substitution in the photosynthetic oxygen-evolving complex, *Biochemistry 41*, 5844−5853.
46. Kimura, Y., Hasegawa, K., Yamanari, T., and Ono, T. (2005) Studies on photosynthetic oxygen-evolving complex by means of Fourier transform infrared spectroscopy: calcium and chloride cofactors, *Photosynth. Res. 84*, 245−250.
47. Strickler, M. A., Walker, L. M., Hillier, W., and Debus, R. J. (2005) Evidence from biosynthetically incorporated strontium and FTIR difference spectroscopy that the C-terminus of the D1 polypeptide of photosystem II does not ligate calcium, *Biochemistry 44*, 8571−8577.
48. Barry, B. A., Hicks, C., De Riso, A., and Jenson, D. L. (2005) Calcium ligation in photosystem II under inhibiting conditions, *Biophys. J. 89*, 393−401.
49. De Riso, A., Jenson, D. L. and Barry, B. A. (2006) Calcium exchange and structural changes during the photosynthetic oxygen evolving cycle, *Biophys. J. 91*, 1999−2008.
50. Sugiura, M., and Inoue, Y. (1999) Highly purified thermo-stable oxygen-evolving photosystem II core complex from the thermophilic cyanobacterium *Synechococcus elongatus* having his-tagged CP43, *Plant Cell Physiol. 40*, 1219−1231.
51. Berthold, D. A., Babcock, G. T., and Yocum, C. F. (1981) A highly resolved, oxygen-evolving photosystem II preparation from spinach thylakoid membranes. EPR and electron-transport properties, *FEBS Lett. 134*, 231−234.
52. Ono, T., and Inoue, Y. (1986) Effects of removal and reconstitution of the extrinsic 33, 24 and 16 kDa proteins on flash oxygen yield in photosystem II particles, *Biochim. Biophys. Acta 850*, 380−389.
53. Ono, T., and Inoue, Y. (1988) Discrete extraction of the Ca atom functional for O_2 evolution in higher plant photosystem II by a simple low pH treatment, *FEBS Lett. 227*, 147−152.
54. Ono, T., Izawa, S., and Inoue, Y. (1992) Structural and functional modulation of the manganese cluster in Ca^{2+}-depleted photosystem II induced by binding of the 24-kilodalton extrinsic protein, *Biochemistry 31*, 7648−7655.
55. Hienerwadel, R., and Berthomieu, C. (1995) Bicarbonate binding to the non-heme iron of photosystem II investigated by FTIR difference spectroscopy and ^{13}C-labeled bicarbonate, *Biochemistry 34*, 16288−16297.
56. Noguchi, T., and Inoue, Y. (1995) Identification of FTIR signals from the non-heme iron in photosystem II, *J. Biochem. 118*, 9−12.
57. Zimmermann, J.-L., and Rutherford, A. W. (1986) Photoreductant-induced oxidation of Fe^{2+} in the electron-acceptor complex of photosystem II, *Biochim. Biophys. Acta 851*, 416−423.
58. Petrouleas, V., and Diner, B. A. (1987) Light-induced oxidation of the acceptor-side Fe(II) of photosystem II by exogenous quinones acting through the Q_B binding site. I. Quinones, kinetics and pH-dependence, *Biochim. Biophys. Acta 893*, 126−137.
59. Hienerwadel, R., Boussac, A., Breton, J., and Berthomieu, C. (1996) Fourier transform infrared difference study of $tyrosine_D$ oxidation and plastoquinone Q_A reduction in photosystem II, *Biochemistry 35*, 15447−15460.
60. Smith, J. C., Gonzalez-Vergara, E., and Vincent, J. B. (1997) Detection of structural changes upon oxidation in multinuclear Mn-oxo-carboxylate assemblies by Fourier transform infrared spectroscopy: relationship to photosystem II, *Inorg. Chim. Acta 255*, 99−103.
61. Kimura, Y., and Ono, T. (2001) Chelator-induced disappearance of carboxylate stretching vibrational modes in S_2/S_1 FTIR spectrum in oxygen-evolving complex of photosystem II, *Biochemistry 40*, 14061−14068.
62. Riggs-Gelasco, P. J., Mei, R., Ghanotakis, D. F., Yocum, C. F., and Penner-Hahn, J. E. (1996) X-ray absorption spectroscopy of calcium-substituted derivatives of the oxygen-evolving complex of Phostosytem II, *J. Am. Chem. Soc. 118*, 2400−2410.

BI061232Z